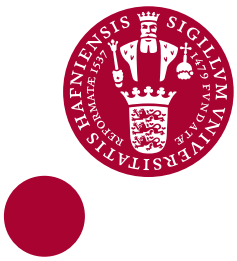

Laboratory spectroscopic study of the 15N isotopomers of cyanamide, H2NCN, and a search for them toward IRAS 16293-2422B

Coutens, Audrey; Zakharenko, Olena; Lewen, Frank; Jorgensen, Jes K.; Schlemmer, Stephan; Mueller, Holger S. P.

Published in:
Astronomy & Astrophysics

DOI:
10.1051/0004-6361/201834605

Publication date:
2019

Document version
Publisher's PDF, also known as Version of record

A&A 623, A93 (2019)
https://doi.org/10.1051/0004-6361/201834605

Astronomy & Astrophysics

Laboratory spectroscopic study of the ^{15}N isotopomers of cyanamide, H_2NCN, and a search for them toward IRAS 16293−2422 B⋆

Audrey Coutens[1], Olena Zakharenko[2], Frank Lewen[2], Jes K. Jørgensen[3], Stephan Schlemmer[2], and Holger S. P. Müller[2]

[1] Laboratoire d'Astrophysique de Bordeaux, Univ. Bordeaux, CNRS, B18N, Allée Geoffroy Saint-Hilaire, 33615 Pessac, France
e-mail: audrey.coutens@u-bordeaux.fr
[2] I. Physikalisches Institut, Universität zu Köln, Zülpicher Str. 77, 50937 Köln, Germany
e-mail: hspm@ph1.uni-koeln.de
[3] Centre for Star and Planet Formation, Niels Bohr Institute and Natural History Museum of Denmark, University of Copenhagen, Øster Voldgade 5–7, 1350 Copenhagen K, Denmark

Received 8 November 2018 / Accepted 20 December 2018

ABSTRACT

Context. Cyanamide is one of the few interstellar molecules containing two chemically different N atoms. It was detected recently toward the solar-type protostar IRAS 16293−2422 B together with $H_2N^{13}CN$ and HDNCN in the course of the Atacama Large Millimeter/submillimeter Array (ALMA) Protostellar Interferometric Line Survey (PILS). The detection of the ^{15}N isotopomers or the determination of upper limits to their column densities was hampered by the lack of accurate laboratory data at the frequencies of the survey.
Aims. We wanted to determine spectroscopic parameters of the ^{15}N isotopomers of cyanamide that are accurate enough for predictions well into the submillimeter region and to search for them in the PILS data.
Methods. We investigated the laboratory rotational spectra of $H_2^{15}NCN$ and $H_2NC^{15}N$ in the selected region between 192 and 507 GHz employing a cyanamide sample in natural isotopic composition. Additionally, we recorded transitions of $H_2N^{13}CN$.
Results. We obtained new or improved spectroscopic parameters for the three isotopic species. Neither of the ^{15}N isotopomers of cyanamide were detected unambiguously in the PILS data. Two relatively clean lines can be tentatively assigned to $H_2^{15}NCN$. If confirmed, their column densities would imply a low $^{14}N/^{15}N$ ratio for cyanamide toward this source.
Conclusions. The resulting line lists should be accurate enough for observations up to about 1 THz. More sensitive observations, potentially at different frequencies, may eventually lead to the astronomical detection of these isotopic species.

Key words. molecular data – methods: laboratory: molecular – techniques: spectroscopic – radio lines: ISM – ISM: molecules – astrochemistry

1. Introduction

Cyanamide, H_2NCN, is one of the few interstellar molecules that contain two chemically inequivalent N atoms[1]. It was among the molecules detected early in the interstellar medium (ISM) by radio astronomical means (Turner et al. 1975). The detection was made toward the prolific high-mass star-forming region Sagittarius (Sgr) B2, which is close to the Galactic center. There is also a report on the detection of H_2NCN toward the nearby Orion-KL region (White et al. 2003) and the high-mass protostar IRAS 20126+410 (Palau et al. 2017). Cyanamide was also found in two nearby starburst galaxies NGC 253 (Martín et al. 2006) and M82 (Aladro et al. 2011).

Coutens et al. (2018) reported the first detection of H_2NCN toward two solar-type protostars; one was IRAS 16293−2422 B with the Atacama Large Millimeter/submillimeter Array (ALMA) in the framework of the Protostellar Interferometric Line Survey (PILS), and the other was NGC 1333 IRAS2A in the course of Plateau de Bure Interferometer (PdBI) observations. More recently, a tentative detection was also reported toward the low-mass protostellar source Barnard 1b (Marcelino et al. 2018).

Isotopic fractionation in the N isotopes has attracted considerable interest in recent years. Very different $^{14}N/^{15}N$ ratios have been determined in star-forming regions which range from less than 100 to around 1000 (e.g., Milam & Charnley 2012; Bizzocchi et al. 2013; Wampfler et al. 2014), compared to the terrestrial ratio of 272 (Berglund & Wieser 2011). However, the reasons for the enrichment or depletion in ^{15}N are not clear at present.

In order to address the possible N-fractionation for cyanamide, reliable transition frequencies of these rarer isotopologs are critical. The laboratory rotational spectrum of the

⋆ Transition frequencies for each isotopic species are only available at the CDS via anonymous ftp to cdsarc.u-strasbg.fr (130.79.128.5) or via http://cdsarc.u-strasbg.fr/viz-bin/qcat?J/A+A/623/A93

[1] The other are N_2H^+, N_2O, aminoacetonitrile (NH_2CH_2CN), a heavy homolog of cyanamide, and *E*-cyanomethanimine (*E*-HNCHCN), see e.g., the Molecules in Space page (https://cdms.astro.uni-koeln.de/classic/molecules; note that this link, as well as those in footnotes 3 and 4, are temporarily unavailable. They should be redirected in the near future) of the Cologne Database for Molecular Spectroscopy (Endres et al. 2016), or the list of Interstellar and Circumstellar Molecules of the Astrochymist page (http://www.astrochymist.org/astrochymist_ism.html).

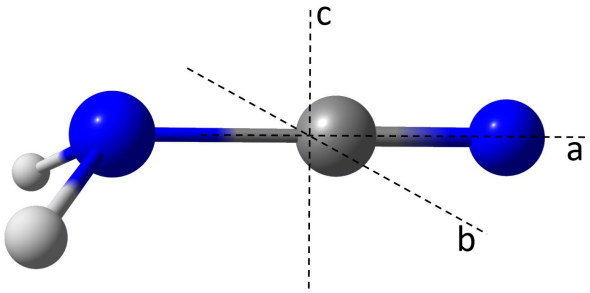

Fig. 1. Schematic representation of the cyanamide molecule; C and N atoms are indicated by gray and blue spheres, respectively, and H atoms by smaller, light gray spheres. The approximate positions of the inertial axes are represented by dashed lines. We note that the C atom is very close to the center of mass and the N atoms are very close to the *a*-axis.

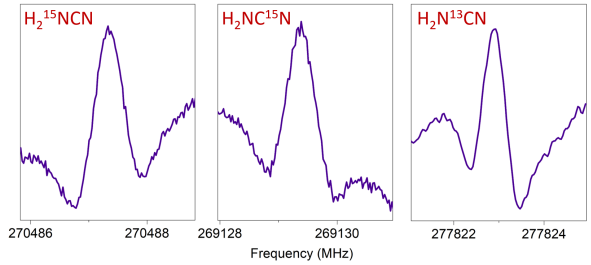

Fig. 2. Sections of the rotational spectrum of cyanamide displaying the $J_{K_a,K_c} = 14_{1,14}-13_{1,13}$ transitions of three isotopic species within the 0^- tunneling state.

H_2NCN main isotopolog has been studied extensively since the fairly early days of microwave spectroscopy (Tyler et al. 1959), especially by Read et al. (1986) and by Birk et al. (1993). Only very limited information was available for minor isotopologs of cyanamide (Tyler et al. 1972; Brown et al. 1985) until fairly recently when Kraśnicki et al. (2011) reported millimeter and in part submillimeter transition frequencies for numerous isotopic species. Kisiel et al. (2013) presented updated accounts on H_2NCN, HDNCN, and D_2NCN. The line lists of the ^{15}N isotopomers covered 135−176 GHz ($J'' = 6-8$) besides some older, lower-accuracy data with $J'' = 0$ or 1 (Kraśnicki et al. 2011). Therefore, we decided to record rotational transitions of $H_2^{15}NCN$ and $H_2NC^{15}N$ between 192 and 507 GHz which should be sufficient to search for these isotopic species throughout the entire presently available frequency range of ALMA up to almost 1 THz. In the course of our measurements, we also recorded some transitions of $H_2N^{13}CN$ to improve its spectroscopic parameters somewhat.

2. Spectroscopic properties of cyanamide

Cyanamide is an asymmetric rotor with $\kappa = (2B - A - C)/(A - C) = -0.9983$, very close to the symmetric limit of −1. A model of the molecule is shown in Fig 1. It is nonplanar with two equivalent configurations, albeit with a low barrier to planarity (Kisiel et al. 2013). Tunneling between the two minima lifts the degeneracy and creates tunneling substates 0^+ and a 0^- which are separated by 1486 GHz (or 49.57 cm^{-1} or 71.32 K). The symmetry of the planar transition state is C_{2v} with the *a*-axis being the symmetry axis. The spin-statistics of the two equivalent H nuclei lead to ortho and para states with a spin-statistical weight ratio of 3:1. The ortho states are described by K_a being even in 0^+ and odd in 0^-. Transitions within the tunneling states obey *a*-type selection rules with $\mu_a(0^+) = (4.25 \pm 0.02)$ D and $\mu_a(0^-) = (4.24 \pm 0.02)$ D (Brown et al. 1985). Tunneling occurs along the *c*-inertial axis, hence the two tunneling states are connected by *c*-type transitions with $\mu_c = (0.91 \pm 0.02)$ D (Brown et al. 1985).

Carbon has two stable isotopes with mass numbers 12 and 13; the terrestrial abundances of the latter is 1.11% (Berglund & Wieser 2011). The corresponding abundance of ^{15}N is 0.36%, much less than the dominant ^{14}N.

3. Laboratory spectroscopic details and observed lines

The investigations of isotopic cyanamide were carried out in a five-meter long double-path glass cell at room temperature and under slow flow conditions. A commercial sample from Sigma-Aldrich was used without further purification. The sample required slight heating to reach a sufficient vapor pressure which was maintained at about 0.5 Pa inside the cell. We employed three frequency multipliers (Virginia Diodes, Inc.) driven by an Agilent E8257D synthesizer as sources with appropriate Schottky diodes as detectors to cover frequencies between 192 and 507 GHz. Frequency modulation reduces standing waves, and the demodulation at twice the modulation frequency leads to approximately second-derivative line-shapes. Further details on the spectrometer system are available in Martin-Drumel et al. (2015).

We optimized the conditions, measurement time, pressure, and modulation deviation, by recording selected transitions of $H_2N^{13}CN$ with K_a values of 1 and 2 around 300 GHz which were well predicted by the available data (Kraśnicki et al. 2011). An integration time of 60 ms per measurement point of one scan upward in frequency and one downward was sufficient for these lines and most of the ^{15}N isotopomers. Several scans were coadded for some weaker lines.

The available $H_2^{15}NCN$ and $H_2NC^{15}N$ transition frequencies obeyed *a*-type selection rules ($\Delta K_a = 0$ and $\Delta K_c = 1$). They covered $J = 7-6$ to $9-8$ with $K_a \leq 5$ and 4 for 0^+ and 0^-, respectively, from Kraśnicki et al. (2011), and some $J = 1-0$ and $2-1$ transitions from Tyler et al. (1972) and Brown et al. (1985). The resulting spectroscopic parameters were good enough to find transitions with low values of J, starting with $10-9$ around 195 GHz and low values of K_a. We determined new spectroscopic parameters and covered several higher J up to $26-25$ near 505 GHz. The K_a range extended eventually to 7 and 6 for 0^+ and 0^-, respectively. The uncertainties ranged from 20 kHz for isolated lines with symmetric line shape and good signal-to-noise ratio to 100 kHz.

Subsequently, we recorded $H_2N^{13}CN$ transitions to supplement earlier measurements by Kraśnicki et al. (2011). Their data included $J = 6-5$ to $8-7$ and $29-28$ to $32-31$ with $K_a \leq 5$ and 6 for 0^+ and 0^-, respectively, at frequencies of 119 to 161 and 578 to 641 GHz. Our data covered $J = 13-12$ to $25-24$ and mostly higher K_a values, 6 for 0^- and 7 for 0^+ and 0^-, along with some lower-K_a data. We assigned uncertainties of 20 or 30 kHz to our $H_2N^{13}CN$ transition frequencies. Figure 2 displays the 0^-, $J_{K_a,K_c} = 14_{1,14}-13_{1,13}$ transition of each of the three isotopologs.

4. Determination of spectroscopic parameters

We used Pickett's SPCAT and SPFIT programs (Pickett 1991) to predict and fit rotational spectra of the minor isotopic species of cyanamide employing the reduced axis system Hamiltonian (Pickett 1972), as was done previously (Read et al. 1986; Birk et al. 1993; Kraśnicki et al. 2011; Kisiel et al. 2013). We

used Watson's S reduction of the rotational Hamiltonian, in contrast to the latest two publications but in agreement with earlier work. Noting that the ground vibrational state $v = 0$ consists of the substates 0^+ and 0^-, we fit average spectroscopic parameters $X = (X(0^+) + X(0^-))/2$ and $\Delta X = X(0^-) - X(0^+)$, as proposed by Christen & Müller (2003). The model was tested for the rotational spectrum of NH_2D and applied successfully in an analysis of the rotational and rovibrational spectra of H_2DO^+ (Müller et al. 2010). The advantage of being able to add parameters or their differences separately was particularly apparent in the case of ethanethiol (Müller et al. 2016). As the available experimental lines of the minor isotopic species are considerably smaller than those of the main species, we estimated several of the higher-order parameters of the former by scaling parameters of the main isotopolog by the ratios of appropriate powers of $A - (B + C)/2$, $B + C$, and $B - C$, as done recently for $H_2C^{16}O$, $H_2C^{17}O$, and $H_2C^{18}O$ (Müller & Lewen 2017). A similar approach was taken for fitting spectra of isotopic species of cyanamide (Kraśnicki et al. 2011).

Our reanalysis of H_2NCN data started with the line list from Kisiel et al. (2013). The very extensive line list was not reproduced within experimental uncertainties on average, such that the authors omitted transitions with residuals between observed transition frequencies and those calculated from the final set of spectroscopic parameters exceeding three times the uncertainties. Initially, we weighted down these lines, but omitted most of them in the end because the residuals in our final fit were very similar to those of the previous fit. In fact, our final parameter set differed effectively only slightly from that obtained by Kisiel et al. (2013). We added fixed values of L_K and ΔL_K to account better for transitions higher in K_a, especially c-type transitions between the tunneling states. The parameter values were obtained from a fit to the line list deposited in the JPL catalog archive (Pickett et al. 1998) which was based on Read et al. (1986) and Birk et al. (1993) and which extended to transitions considerably higher in K_a. In addition, we did not use ΔL_{JK} in the fit. Our parameter values were in good agreement with those of Kisiel et al. (2013), as was expected. The majority of their transition frequencies were obtained by far-infrared spectroscopy. They were reproduced on average to ~0.00023 cm^{-1}, slightly above the reported uncertainties of ~0.00020 cm^{-1}. Therefore, we increased the uncertainties to ~0.00025 cm^{-1}. The parameter values changed little, but now not only the frequencies determined with microwave accuracy were reproduced within uncertainties on average, but also the far-infrared transition frequencies.

The details for determining spectroscopic parameters were the same for the two ^{15}N isotopomers of cyanamide and for $H_2N^{13}CN$. The parameter set of the main isotopic species was taken as a start. Low-order spectroscopic parameters were fit until the transition frequencies were reproduced within around five times the experimental uncertainties. At each step, we searched for the parameter which improved the quality of the fit the most. Subsequently, parameters still kept fixed were scaled with appropriate powers of the ratios of $B+C$ and $B-C$. Since A was correlated with ΔE, scaling with appropriate powers of the ratios of $A - (B + C)/2$ was done subsequently; ΔA was scaled with the ratio of A; the distortion corrections to F_{ac} were scaled in addition with the ratios of the F_{ac}. In the next step, parameters of higher order were released until the qualities of the fits no longer significantly improved. In a final step, ΔA was scaled again with the ratio of A. Kraśnicki et al. (2011) assigned uncertainties of 50 kHz to their transition frequencies. These were appropriate in the case of the ^{15}N isotopomers. In the case of $H_2N^{13}CN$, they were slightly pessimistic at lower frequencies (119−161 GHz) and slightly optimistic at higher frequencies (578−644 GHz). Uncertainties of 30 and 60 kHz, respectively, turned out to be appropriate. Uncertainties of 100 kHz were used for the few older transition frequencies (Tyler et al. 1972; Brown et al. 1985). The transition frequencies of each isotopic species as well as subsets thereof were reproduced mostly within and always close to the experimental uncertainties on average. The resulting spectroscopic parameters are given in Table 1 together with those of the main isotopic species. The experimental line lists have been deposited at the Centre de Données astronomiques de Strasbourg (CDS) as three separate ascii files. A portion is shown for one isotopolog in Table A.1.

The line lists are quite similar in quantum number coverage among the three minor isotopic species and even more so among the two ^{15}N isotopomers. Therefore, it is not so surprising that the parameters determined in the fits are the same and their respective uncertainties are quite similar. Some smaller uncertainties of specific $H_2N^{13}CN$ parameters compared to those of the ^{15}N species are a consequence of lines with higher values of J (Kraśnicki et al. 2011). Our initial fits of the old data are summarized in Table B.1 together with our new parameters for $H_2N^{13}CN$. The uncertainties of all parameters improved slightly upon addition of our experimental data. The main aspect in case of the two ^{15}N isotopomers is the increase of determined spectroscopic parameters from ten to 22 because of the increase in J from 9 to 26 and in K_a from 5 to 7. The spectroscopic parameters included in the fit are equivalent to those of Kraśnicki et al. (2011); similar to that work, values for A, D_K, and so on were taken from the main isotopic species and the remaining parameters were estimated as described above.

It is also not surprising that the NH_2 tunneling splitting is not affected within uncertainties by substituting the distant cyano-N atom, only marginally affected by substitution of the closer cyano-C atom, and somewhat more by the substitution of the amino-N atom. Replacing one or both of the H atoms by D affects the tunneling splitting much more (Kisiel et al. 2013). The heavy atoms are all located close to the a-axis, see Fig. 1 in Kraśnicki et al. (2011), hence heavy atom substitutions do not change the A rotational parameter much. In addition, the C atom is quite close to the center of mass of the molecule such that its substitution changes B and C only slightly whereas replacing one of the N atoms cause larger changes. Changes in higher order spectroscopic parameters often reflect the changes in $B+C$ and $B-C$, but exceptions occur, especially for some of the higher order parameters.

5. Astronomical search

We used the ALMA PILS data to search for the ^{15}N isotopomers of cyanamide. PILS is an unbiased molecular line survey of the Class 0 protostellar binary IRAS 16293−2422 carried out in band 7 of ALMA and covering the spectral range 329.15−362.90 GHz at 0.244 MHz resolution (project-id: 2013.1.00278.S, PI: Jes K. Jørgensen[2]). Details of the survey have been presented by Jørgensen et al. (2016). The spectral sensitivity is also very high, 7−10 mJy $beam^{-1}$ $channel^{-1}$ or 4−5 mJy $beam^{-1}$ $km\,s^{-1}$ such that line confusion is reached in considerable parts of the survey. This high sensitivity is very important for searching for less abundant molecules or for minor isotopic species of somewhat more abundant molecules. Many of our analyses focused on source B because of its smaller line widths of ~1 $km\,s^{-1}$ compared to around 3 $km\,s^{-1}$

[2] http://youngstars.nbi.dk/PILS/

Table 1. Spectroscopic parameters X^a (MHz) and their differences ΔX^b (MHz) of cyanamide isotopologs.

Parameter	$H_2^{15}NCN$	$H_2NC^{15}N$	$H_2N^{13}CN$	H_2NCN
ΔE	1460174. (120)	1486116. (118)	1486522. (66)	1486004.275 (185)
F_{ac}	342.505 (46)	335.828 (47)	345.963 (59)	346.5304 (245)
F_{ac}^{K}	−1.442	−1.415	−1.457	−1.4577 (40)
$F_{ac}^{J} \times 10^3$	1.2756 (113)	1.1048 (119)	1.2514 (108)	1.2009 (89)
$F_{ac}^{JK} \times 10^6$	−48.69	−47.52	−50.54	−50.57 (155)
$F_{ac}^{JJ} \times 10^9$	10.64	10.32	11.34	11.36 (48)
A	307819.7 (241)	308328.7 (239)	308205.1 (122)	308298.054 (66)
$\Delta A/2$	−3838.00	−3844.35	−3842.81	−3843.971 (33)
B	9845.11174 (75)	9794.54528 (82)	10117.07868 (93)	10121.205258 (188)
$\Delta B/2$	−8.74933 (71)	−8.09439 (79)	−8.56394 (93)	−8.551540 (113)
C	9604.18856 (76)	9555.59774 (79)	9862.34933 (114)	9866.291773 (186)
$\Delta C/2$	−0.28904 (77)	−0.26534 (81)	−0.35051 (110)	−0.368180 (109)
D_K	36.036	36.110	36.070	36.0421 (44)
$\Delta D_K/2$	−8.084	−8.101	−8.092	−8.0857 (33)
$D_{JK} \times 10^3$	368.428 (80)	357.939(80)	377.325 (101)	377.705 (40)
$\Delta D_{JK}/2 \times 10^3$	−19.239 (44)	−17.766 (42)	−18.097 (83)	−18.494 (26)
$D_J \times 10^3$	3.59457 (39)	3.50397 (38)	3.75968 (31)	3.759689 (180)
$\Delta D_J/2 \times 10^3$	0.01490 (34)	0.01741 (32)	0.01813 (26)	0.018511 (49)
$d_1 \times 10^6$	−126.84 (48)	−117.29 (49)	−129.70 (36)	−130.2699 (176)
$\Delta d_1/2 \times 10^6$	8.89 (47)	9.37 (49)	10.88 (36)	10.5633 (225)
$d_2 \times 10^6$	−25.100 (283)	−23.484 (304)	−27.739 (219)	−27.2965 (45)
$\Delta d_2/2 \times 10^6$	4.931 (150)	4.062 (206)	5.516 (165)	5.2987 (43)
$H_K \times 10^3$	10.76	10.79	10.77	10.760 (84)
$\Delta H_K/2 \times 10^3$	−6.45	−6.47	−6.46	−6.453 (78)
$H_{KJ} \times 10^6$	−219.2 (50)	−267.7 (48)	−196.2 (45)	−264.41 (234)
$\Delta H_{KJ}/2 \times 10^6$	71.6 (12)	70.6 (10)	82.3 (7)	73.64 (180)
$H_{JK} \times 10^6$	0.889 (73)	1.115 (70)	0.945 (44)	1.0798 (167)
$\Delta H_{JK}/2 \times 10^6$	−0.250 (27)	−0.268 (23)	−0.297 (11)	−0.2879 (65)
$H_J \times 10^9$	−0.761	−0.750	−0.825	−0.826 (77)
$\Delta H_J/2 \times 10^9$	0.189	0.186	0.204	0.205 (9)
$L_K \times 10^6$	16.00	16.07	16.04	16.01
$\Delta L_K/2 \times 10^6$	−5.31	−5.34	−5.32	−5.32
$L_{KKJ} \times 10^6$	−4.118 (88)	−3.439 (82)	−5.800 (54)	−3.681 (46)
$\Delta L_{KKJ}/2 \times 10^6$	0.343	0.343	0.353	0.353 (39)
$L_{JK} \times 10^9$	17.78 (223)	10.10 (199)	17.44 (94)	12.47 (42)
rms	0.040	0.037	0.043	0.098
σ^b	0.82	0.86	0.98	0.94

Notes. Watson's S reduction has been used in the representation I^r. [(a)]Numbers in parentheses are one standard deviation in units of the least significant figures. Parameters without uncertainties were estimated and kept fixed in the analyses. $X = (X(0^+) + X(0^-))/2$ and $\Delta X = X(0^-) - X(0^+)$. [(b)]Reduced standard deviation (unitless).

for source A. Among the most exciting results was the detection of methyl chloride toward both sources as the first interstellar organohalogen compound (Fayolle et al. 2017) besides numerous isotopologs containing D or ^{13}C, many of them for the first time in space (Coutens et al. 2016, 2018; Jørgensen et al. 2018, 2016; Persson et al. 2018; Calcutt et al. 2018).

Coutens et al. (2018) analyzed column densities of cyanamide isotopologs toward a position offset by 0.5″ from the continuum peak of source B (α_{J2000} = 16^{h}32^{m}22.^{s}58, δ_{J2000} = −24°28′32.8″). This position was chosen to minimize the effects of line self-absorption, which was particularly prominent for the main isotopolog of cyanamide. The emission lines were modeled under the assumption of local thermodynamic equilibrium, which is reasonable at the high densities and high temperatures of source B, with an excitation temperature T_{ex} = 300 K, a source size of 0.5″, and a full line width at half maximum (FWHM) of 1 km s^{-1}. A column density of 7×10^{13} cm^{-2} was obtained for the $H_2N^{13}CN$ isotopolog. Assuming a standard $^{12}C/^{13}C$ ratio, the abundance of the main isotopolog is about 4.8×10^{15} cm^{-2}.

As a result of our spectroscopic investigation, we can now search for the ^{15}N isotopomers of cyanamide with confidence. The molecules have several lines in the range of PILS, but most of them were well below the limit of detection or, in some cases, blended with bright lines of other species. We find two lines that can potentially be assigned to $H_2^{15}NCN$ (see Fig. 3) and none for $H_2NC^{15}N$. We carefully checked that the two potential lines of $H_2^{15}NCN$ were not due to any other species already identified toward this source and that no line expected to be observed was missing. Using the same position, T_{ex}, source size, and FWHM as for H_2NCN, we obtain a good model for a column density of 6×10^{13} cm^{-2} (see Fig. 3). As the spectra of IRAS 16293−2422

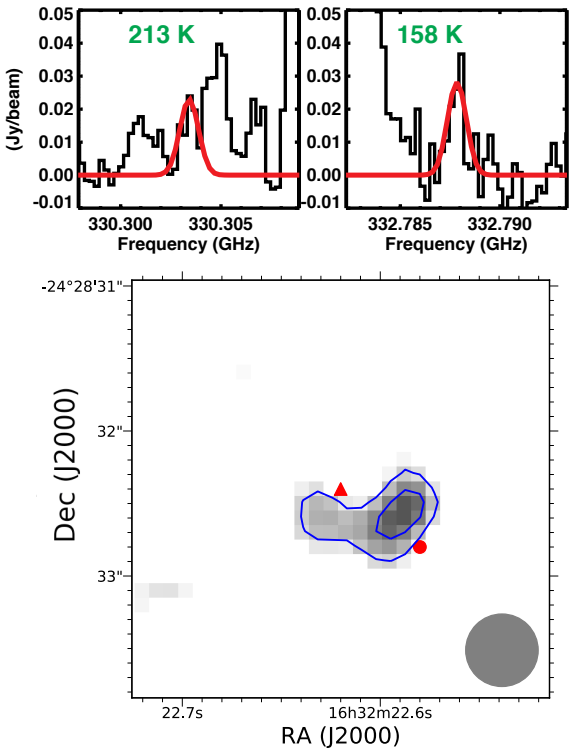

Fig. 3. *Upper panels*: sections of the Protostellar Interferometric Line Survey toward a position one beam offset from source B displaying two potential lines of $H_2^{15}NCN$. The model described in Sect. 5 is indicated in red. The E_{up} values of the two transitions are indicated in green in the upper part of each panel. *Lower panel*: integrated intensity map of the transition at 322.7878 GHz. The blue contours correspond to 5 and 7σ. The red triangle indicates the position of the continuum peak position, while the red circle indicates the position we analyzed (one beam offset).

are very line-rich, more transitions need to be detected to claim a secure detection. For now, this column density can only be considered as an upper limit. A 3σ upper limit of 3×10^{13} cm^{-2} is derived for $H_2NC^{15}N$. This corresponds to $^{14}N/^{15}N$ ratios of $\gtrsim$80 for $H_2^{15}NCN$ and $\gtrsim$160 for $H_2NC^{15}N$. For comparison in the same source, the $^{14}N/^{15}N$ ratio of CH_3CN is about 250 (Calcutt et al. 2018), while a similar lower limit of 100 was derived for NH_2CHO (Coutens et al. 2016). Single-dish observations of two and one transitions of HCN and HNC isotopologs led to ratios of 163 ± 20, 190 ± 38, and 242 ± 32, respectively (Wampfler et al. 2014).

More sensitive observations are required to confirm the detection of $H_2^{15}NCN$ and possibly identify $H_2NC^{15}N$ in IRAS 16293−2422. Such observations may be more promising at lower frequencies because line blending and issues due to absorption are likely smaller. In addition, observations are, for the most part, easier at lower frequencies. On the other hand, the intensities of cyanamide emission drop fast at lower frequencies. Therefore, we inspected a synthetic spectrum of the 200−320 GHz region for bright lines of the ^{15}N isotopomers of cyanamide that are not blended with lines of species in a synthetic spectrum which includes most of the species identified in the PILS data with certainty. About 20 lines of $H_2^{15}NCN$ and less than 10 lines of $H_2NC^{15}N$ are currently predicted to be free of blending. Since most of the blends in the PILS Band 7 data are caused by known species, it may well be that a fair fraction of the about 30 lines of cyanamide containing ^{15}N will eventually turn out to be unblended.

6. Conclusion and outlook

Our studies of isotopic cyanamide yielded greatly extended experimental line lists of $H_2^{15}NCN$ and $H_2NC^{15}N$ up to 507 GHz. The resulting spectroscopic parameters should permit sufficiently accurate extrapolation in J up to ~1 THz, that is, throughout all presently available ALMA bands. Extrapolation in K_a may be questionable because of vibration-rotation interaction, but the covered range should be sufficient for all minor isotopic species. Transitions between the tunneling states, which obey c-type selection rules, cannot be predicted with meaningful accuracy. These transitions are quite weak and have, to the best of our knowledge, not been identified in space even for the main isotopic species. The line list of $H_2N^{13}CN$ has been extended somewhat in the course of the present investigation, and the spectroscopic parameters have been improved.

Calculated line lists of these three isotopic species, including information on their intensities and their calculated uncertainties, will be provided or updated in the catalog section[3] of the Cologne Database for Molecular Spectroscopy, CDMS (Endres et al. 2016). Files containing the experimental lines or parameters along with auxiliary files are available in the data section of the CDMS[4].

A first attempt to search for the ^{15}N isotopologs of cyanamide in the PILS data turned out to be negative. The two lines assignable to $H_2^{15}NCN$ would imply a low $^{14}N/^{15}N$ ratio if their identity were to be confirmed. Future, more sensitive observations of IRAS 16293−2422 are required to improve the upper limits or even lead to an unambiguous detection of at least one of the isotopic species.

Acknowledgements. The measurements in Köln were supported by the Deutsche Forschungsgemeinschaft (DFG) in the framework of the collaborative research grant SFB 956, project B3. A.C.'s postdoctoral grant is funded by the ERC Starting Grant 3DICE (grant agreement 336474) under the European Union's Horizon 2020 research and innovation program. A.C. is grateful to COST (European Cooperation in Science and Technology) for a STSM grant from the COST Action CM1401 "Our Astro-Chemical History". O.Z. is funded by the DFG via the Gerätezentrum "Cologne Center for Terahertz Spectroscopy". The research of J.K.J. is supported by the European Research Council through the ERC Consolidator Grant "S4" (grant agreement No 646908) and Centre for Star and Planet Formation funded by the Danish National Research Foundation. This paper makes use of the following ALMA data: ADS/JAO.ALMA#2013.1.00278.S. ALMA is a partnership of ESO (representing its member states), NSF (USA) and NINS (Japan), together with NRC (Canada), NSC and ASIAA (Taiwan), and KASI (Republic of Korea), in cooperation with the Republic of Chile. The Joint ALMA Observatory is operated by ESO, AUI/NRAO and NAOJ. Our research benefited from NASA's Astrophysics Data System (ADS).

References

Aladro, R., Martín, S., Martín-Pintado, J., et al. 2011, A&A, 535, A84
Belloche, A., Müller, H. S. P., Menten, K. M., Schilke, P., & Comito, C. 2013, A&A, 559, A47
Berglund, M., & Wieser, M. E. 2011, Pure Appl. Chem., 83, 397
Birk, M., Winnewisser, M., & Cohen, E. A. 1993, J. Mol. Spectr., 159, 69
Bizzocchi, L., Caselli, P., Leonardo, E., & Dore, L. 2013, A&A, 555, A109
Brown, R. D., Godfrey, P. D., & Kleibömer, B. 1985, J. Mol. Spectr., 114, 257
Calcutt, H., Jørgensen, J. K., Müller, H. S. P., et al. 2018, A&A, 616, A90
Christen, D., & Müller, H. S. P. 2003, Phys. Chem. Chem. Phys., 5, 3600
Coutens, A., Jørgensen, J. K., van der Wiel, M. H. D., et al. 2016, A&A, 590, L6
Coutens, A., Willis, E. R., Garrod, R. T., et al. 2018, A&A, 612, A107
Endres, C. P., Schlemmer, S., Schilke, P., Stutzki, J., & Müller, H. S. P. 2016, J. Mol. Spectr., 327, 95
Fayolle, E. C., Öberg, K. I., Jørgensen, J. K., et al. 2017, Nat. Astron., 1, 703

[3] https://cdms.astro.uni-koeln.de/classic/entries/
[4] https://cdms.astro.uni-koeln.de/classic/predictions/daten/Cyanamide

Jørgensen, J. K., van der Wiel, M. H. D., Coutens, A., et al. 2016, A&A, 595, A117
Jørgensen, J. K., Müller, H. S. P., Calcutt, H., et al. 2018, A&A, 620, A170
Kisiel, Z., Kraśnicki, A., Jabs, W., et al. 2013, J. Phys. Chem. A, 117, 9889
Kraśnicki, A., Kisiel, Z., Jabs, W., Winnewisser, B. P., & Winnewisser, M. 2011, J. Mol. Spectr., 267, 144
Martín, S., Mauersberger, R., Martín-Pintado, J., Henkel, C., & García-Burillo, S. 2006, ApJS, 164, 450
Martin-Drumel, M. A., van Wijngaarden, J., Zingsheim, O., et al. 2015, J. Mol. Spectr., 307, 33
Marcelino, N., Gerin, M., Cernicharo, J., et al. 2018, A&A, 620, A80
Milam, S. N., & Charnley, S. B. 2012, Lunar Planet. Sci. Conf., 43, 2618
Müller, H. S. P., & Lewen, F. 2017, J. Mol. Spectr., 331, 28
Müller, H. S. P., Dong, F., Nesbitt, D. J., Furuya, T., & Saito, S. 2010, Phys. Chem. Chem. Phys., 12, 8362
Müller, H. S. P., Brown, L. R., Drouin, B. J., et al. 2015, J. Mol. Spectr., 312, 22
Müller, H. S. P., Belloche, A., Xu, L.-H., et al. 2016, A&A, 587, A92
Palau, A., Walsh, C., Sánchez-Monge, Á., et al. 2017, MNRAS, 467, 2723
Persson, M. V., Jørgensen, J. K., Müller, H. S. P., et al. 2018, A&A, 610, A54
Pickett, H. M. 1972, J. Chem. Phys., 56, 1715
Pickett, H. M. 1991, J. Mol. Spectr., 148, 371
Pickett, H. M., Poynter, R. L., Cohen, E. A., et al. 1998, J. Quant. Spectr. Rad. Transf., 60, 883
Read, W. G., Cohen, E. A., & Pickett, H. M. 1986, J. Mol. Spectr., 115, 316
Turner, B. E., Liszt, H. S., Kaifu, N., & Kisliakov, A. G. 1975, ApJ, 201, L149
Tyler, J. K., Thomas, L. F., & Sheridan, J. 1959, Proc. Chem. Soc., 12, 250
Tyler, J. K., Sheridan, J., & Costain, C. C. 1972, J. Mol. Spectr., 43, 248
Wampfler, S. F., Jørgensen, J. K., Bizzarro, M., & Bisschop, S. E. 2014, A&A, 572, A24
White, G. J., Araki, M., Greaves, J. S., Ohishi, M., & Higginbottom, N. S. 2003, A&A, 407, 589

Appendix A: Supplementary material

Table A.1. Assigned transitions for $H_2^{15}NCN$, observed transition frequency (MHz), experimental uncertainty Unc. (MHz), residual O−C between observed frequency and that calculated from the final set of spectroscopic parameters, weight for blended lines, and source of line.

J'	K'_a	K'_c	v'_t	J''	K''_a	K''_c	v''_t	Frequency	Unc.	O−C	Weight	
1	0	1	0	0	0	0	0	19458.1	0.1	−0.15777		Tyler et al. (1972)
2	0	2	0	1	0	1	0	38916.282	0.100	0.00717		Brown et al. (1985)
7	0	7	0	6	0	6	0	136194.32870	0.05000	0.00263		Kraśnicki et al. (2011)
8	0	8	0	7	0	7	0	155645.83281	0.05000	−0.01287		Kraśnicki et al. (2011)
9	0	9	0	8	0	8	0	175095.43308	0.05000	−0.00786		Kraśnicki et al. (2011)
21	6	15	1	20	6	14	1	407549.715	0.050	0.05275	0.5000	Koeln
21	6	16	1	20	6	15	1	407549.715	0.050	0.05275	0.5000	Koeln
25	6	19	1	24	6	18	1	485115.812	0.050	0.04584	0.5000	Koeln
25	6	20	1	24	6	19	1	485115.812	0.050	0.04584	0.5000	Koeln
26	6	20	1	25	6	19	1	504502.373	0.030	−0.03347	0.5000	Koeln
26	6	21	1	25	6	20	1	504502.373	0.030	−0.03347	0.5000	Koeln

Notes. This table and those of other isotopologs are available in their entirety at the CDS. A portion is shown here for guidance regarding its form and content. The quantum number designators $v_t = 0$ and 1 indicate the tunneling states 0^+ and 0^-, respectively.

Appendix B: Fits of previous data

Table B.1. Initial spectroscopic parameters X^a (MHz) and their differences ΔX^b (MHz) of cyanamide isotopologs derived from the previously published data.

Parameter	$H_2^{15}NCN$	$H_2NC^{15}N$	$H_2N^{13}CN$	$H_2N^{13}CN$, new
ΔE	1462540. (106)	1486091. (133)	1486783. (96)	1486522. (66)
F_{ac}	342.74 (23)	335.42 (41)	345.999 (69)	345.963 (59)
F_{ac}^K	−1.442	−1.415	−1.457	−1.457
$F_{ac}^J \times 10^3$	1.156	1.125	1.2388 (130)	1.2514 (108)
$F_{ac}^{JK} \times 10^6$	−48.69	−47.52	−50.54	−50.54
$F_{ac}^{JJ} \times 10^9$	10.64	10.32	11.34	11.34
A	308298.	308298.	308209.3 (182)	308205.1 (122)
$\Delta A/2$	−3844.	−3844.	−3842.81	−3842.81
B	9845.1075 (35)	9794.5437 (55)	10117.07913 (141)	10117.07868 (93)
$\Delta B/2$	−8.7495 (36)	−8.0946 (61)	−8.56355 (140)	−8.56394 (93)
C	9604.1941 (33)	9555.5997 (44)	9862.34845 (140)	9862.34933 (114)
$\Delta C/2$	−0.28904 (77)	0.2699 (49)	0.35121 (136)	−0.35051 (110)
D_K	36.042	36.042	36.070	36.070
$\Delta D_K/2$	−8.086	−8.086	−8.092	−8.092
$D_{JK} \times 10^3$	367.767 (92)	358.168(109)	376.911 (169)	377.325 (101)
$\Delta D_{JK}/2 \times 10^3$	−19.186 (139)	−17.628 (168)	−17.972 (102)	−18.097 (83)
$D_J \times 10^3$	3.6056 (207)	3.4887 (218)	3.76075 (44)	3.75968 (31)
$\Delta D_J/2 \times 10^3$	0.0165 (204)	0.0405 (221)	0.01861 (34)	0.01813 (26)
$d_1 \times 10^6$	−119.81	−118.22	−130.23 (44)	−129.70 (36)
$\Delta d_1/2 \times 10^6$	9.71	9.59	10.54 (44)	10.88 (36)
$d_2 \times 10^6$	−24.383	−23.984	−27.119 (280)	−27.739 (219)
$\Delta d_2/2 \times 10^6$	4.733	4.656	5.484 (167)	5.516 (165)
$H_K \times 10^3$	10.76	10.76	10.77	10.77
$\Delta H_K/2 \times 10^3$	−6.45	−6.45	−6.46	−6.46
$H_{KJ} \times 10^6$	−257.	−256.	−235.5 (118)	−196.2 (45)
$\Delta H_{KJ}/2 \times 10^6$	72.	71.	84.4 (32)	82.3 (7)
$H_{JK} \times 10^6$	1.020	1.012	1.122 (86)	0.945 (44)
$\Delta H_{JK}/2 \times 10^6$	−0.273	−0.270	−0.267 (26)	−0.297 (11)
$H_J \times 10^9$	−0.761	−0.750	−0.825	−0.825
$\Delta H_J/2 \times 10^9$	0.189	0.186	0.204	0.204
$L_K \times 10^6$	16.0	16.0	16.04	16.04
$\Delta L_K/2 \times 10^6$	−5.3	−5.3	−5.32	−5.32
$L_{KKJ} \times 10^6$	−3.58	−3.56	−4.953 (239)	−5.800 (54)
$\Delta L_{KKJ}/2 \times 10^6$	0.343	0.343	0.353	0.353
$L_{JK} \times 10^9$	11.8	11.7	12.21 (266)	17.44 (94)
rms	0.039	0.032	0.042	0.043
σ^b	0.61	0.58	0.87	0.98

Notes. Our present data are given for $H_2N^{13}CN$ to allow a direct comparison. Watson's S reduction has been used in the representation I^r. [(a)]Numbers in parentheses are one standard deviation in units of the least significant figures. Parameters without uncertainties were estimated and kept fixed in the analyses. $X = (X(0^+) + X(0^-))/2$ and $\Delta X = X(0^-) - X(0^+)$. [(b)]Reduced standard deviation (unitless).